Preparation of photothermal-chemotherapy nanohybrids by complexation of gold nanorods with polyamidoamine dendrimers having poly(ethylene glycol) and hydrophobic chains

Preparation of photothermal-chemotherapy nanohybrids by complexation of gold nanorods with polyamidoamine dendrimers having poly(ethylene glycol) and hydrophobic chains

Takuya Hashimoto, Eiji Yuba*, Atsushi Harada*, Kenji Kono

Department of Applied Chemistry, Graduate School of Engineering, Osaka Prefecture University, 1-1 Gakuen-cho, Naka-ku, Sakai, Osaka 599-8531, Japan

*Corresponding authors: Eiji Yuba and Atsushi Harada

Department of Applied Chemistry, Graduate School of Engineering,

Osaka Prefecture University, 1-1 Gakuen-cho, Naka-ku, Sakai, Osaka 599-8531, Japan

Tel: +81-72-254-9330; Fax: +81-72-254-9330; yuba@chem.osakafu-u.ac.jp,

harada@chem.osakafu-u.ac.jp

Abstract

Combinations of anticancer drugs and laser hyperthermia could lead to efficient cancer treatment with less-adverse effects. This study combined anticancer drug-loaded functional dendrimers and light-responsive gold nanorods to fabricate nanohybrids that can provide anticancer-drug delivery and subsequent heat generation under near-infrared laser irradiation. A condensation reaction was used to conjugate poly(ethylene glycol)-modified polyamidoamine dendrimers to carboxylated gold nanorod surfaces. Oleoyl groups were incorporated into dendrimers to improve the drug loading capacity. Doxorubicin loading capacity was improved by incorporation of oleoyl chains to dendrimers in the nanohybrid, indicating increased hydrophobic interaction between anticancer drugs and nanohybrids. Nanohybrids exhibited heat generation properties under near infrared laser irradiation. They released anticancer drugs over time. The combination of doxorubicin-loaded nanohybrids and laser irradiation showed markedly better cytotoxicity than those of nanohybrids used with lasers and drug-loaded nanohybrids without the use of lasers. After intravenous or intratumoral injection of nanohybrids to tumor-bearing mice, a sharp temperature increase was observed at the tumor site under laser irradiation. Especially, intratumorally injected doxorubicin-loaded nanohybrids showed almost complete tumor growth suppression under laser irradiation.

Results demonstrate that functional dendrimer–gold nanorod nanohybrids are promising as multi-functional nanomaterials to achieve synergistic effects of anticancer drugs and heat ablation to support effective cancer treatments.
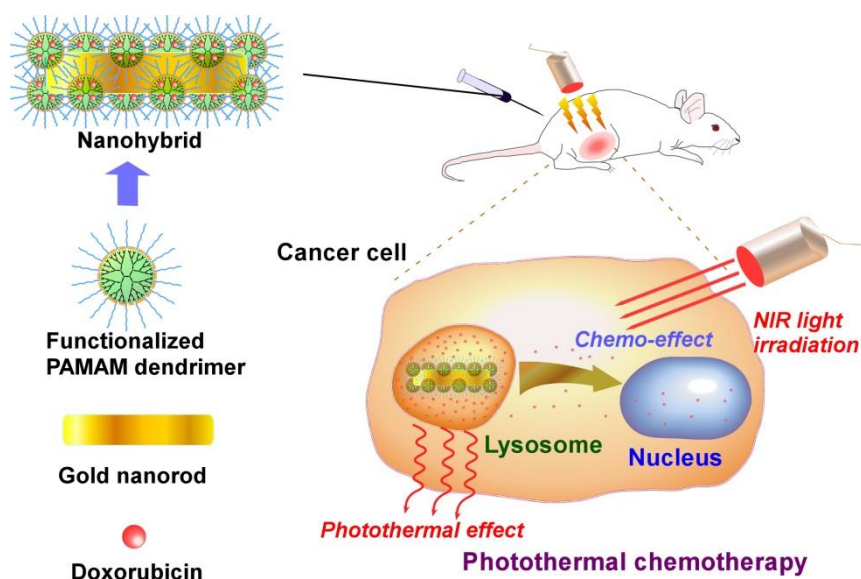
1. Introduction

Establishment of a novel methodology for effective and noninvasive cancer treatments is necessary because common cancer treatments such as surgery, chemotherapy, and radiotherapy often lead to poor prognoses because of insufficient treatment efficacy and severe adverse effects. Laser hyperthermia, by which thermal energy produced by a laser destroys tumors[1], is anticipated as a promising cancer treatment for controlled and site-specific therapy. Unfortunately, nonspecific absorption

attributable to the high laser intensity also damages normal tissues[2,3]. Intended as minimally invasive and localized cancer treatment, plasmonic photothermal therapy (PPTT) using photothermal agents that generate heat under light irradiation has been studied to support laser hyperthermia[4–6]. Superparamagnetic iron oxide nanoparticles (SPIONs)[7], carbon nanomaterials[8,9], and gold nanoparticles[6] are representative photothermal agents used for PPTT.

Treatment using near infrared (NIR) light is particularly regarded as useful for minimally invasive and efficient PPTT because hemoglobin and water have minimal absorption coefficients in the NIR region (650–900 nm)[10,11]. The benefit is great because they are the major absorbers of visible and infrared light.

Among photothermal agents, gold nanorods (AuNR) have unique characteristics that include small size, high efficiency of absorption in the NIR region, and narrower spectral width than other gold nanostructures such as gold nanoshells and gold nanocages, single-walled carbon nanotubes, and polypyrrole and polyaniline nanoparticles[4]. On AuNR, NIR light energy can be converted efficiently to thermal energy through localized surface plasmon resonance (LSPR). That generated heat is useful to kill cancer cells during photothermal treatment. Therefore, AuNR-based nanomedicines have attracted much attention for applications to biomedical fields in recent years[12–18].

To date, functional polymers, DNA, and silica have been conjugated to AuNR to provide colloidal stability or intracellular delivery function and to improve the therapeutic efficacy of drug and gene treatments[19–22]. Especially, AuNRs modified with dendrimers have been investigated for biomedical applications[23]. Dendrimers, which are highly branched macromolecules with defined structures and globular shape, are regarded as a promising nanomaterial because of their potential for molecular design and their capability to encapsulate guest molecules. Modification of functional molecules into terminal amino groups augments dendrimers with various functions that can include biocompability, target specificity, and bioimaging function[24–29]. Drugs can also be conjugated to the terminal groups of dendrimer with linkers such as ester bond, hydrazone bond, disulfide bond, and enzyme-cleavable peptide sequences. Poly(ethylene glycol) (PEG)-modified polyamidoamine (PAMAM) dendrimer–AuNR conjugates having doxorubicin (DOX) through an acid-labile hydrazone bond showed enhanced blood circulation properties and antitumor effects under NIR laser irradiation in our earlier study[30]. For drug conjugation methods, however, multiple synthetic steps are required, leading to a low yield of the final conjugate. In fact, in most cases, the drug molecules must be cleaved in the specified timing and specific site[29]. Instead of drug conjugation that occurs by covalent bonding, drug loading by non-covalent bonding is investigated in

the present study to prepare drug-loaded nanohybrids. Hydrophobic compounds can be

solubilized by dendrimers in an aqueous solution[31]. Reportedly, drug loading to

dendrimers by non-covalent bonding depends on the dendrimer chemical structure. As

one example, because of the stronger hydrophobicity of poly(propylene imine) (PPI) than

that of PAMAM, PPI dendrimers can achieve more effective loading of hydrophobic

drugs than PAMAM dendrimer can[32]. Considering that changing the molecular

framework of a dendrimer itself is not easy, a system that can readily control the

hydrophobicity of dendrimers is needed for a versatile drug nanocarrier. Incorporation

of hydrophobic moiety to PEG-PAMAM dendrimer enables high drug loading capacity[33].

Reportedly, myristic chain-modified PAMAM-dendrimer increases tamoxifen loading

capability[34]. Therefore, the incorporation of hydrophobic moieties into dendrimers is

anticipated as an effective strategy for drug loading improvement.

For this study, AuNR-PAMAM dendrimer nanohybrids having hydrophobic

moieties were prepared (Figure 1). Mercaptohexadecanoic acid (MHA)-modified AuNR

were covered with PAMAM G4 dendrimers having both PEG and oleoyl chains. PEG

increases biocompatibility and stability in blood circulation of dendrimer and AuNRs *in*

vivo[35,36]. Oleoyl chains are expected to improve drug loading capacity by virtue of their

hydrophobic interaction. In the present study, their ability to kill cancer cells *in vitro* and

in vivo was examined to demonstrate the utility of multifunctional nanohybrids for application to cancer treatment.
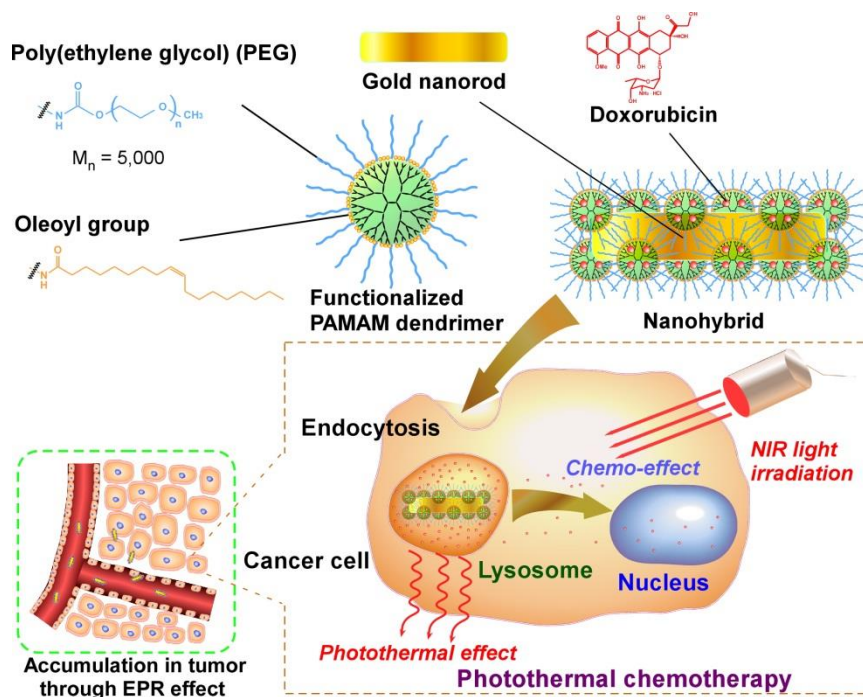

Figure 1. Design of a nanohybrid comprising gold nanorod complexed with PEG/oleoyl group-modified PAMAM dendrimers containing anticancer drugs for photothermal chemotherapy.

2. Experimental section

2.1. Materials.

Hydrogen tetrachloroaurate (III) tetrahydrate (HAuCl$_4$·4H$_2$O), sodium borohydrate (NaBH$_4$), silver nitrate (AgNO$_3$), 3-(4,5-dimethyl-2-thiazoryl)-2,5-diphenyl-2H-tetrazolium bromide (MTT), 1-ethyl-3-(3-dimethylaminopropyl)carbodiimide

hydrochloride (EDC·HCl), N-hydroxysuccinimide (NHS), diethyl ether, toluene,

dichloromethane, and ethanol were purchased from Wako Pure Chemical (Osaka, Japan).

Cetylbutyltrimethylammonium bromide (CTAB), 4th generation PAMAM dendrimer (10

wt% in methanol), α-methoxy-ω-hydroxy-poly(ethylene glycol) (PEG-OH, Mn: 5000),

4-nitrophenyl chloroformate, 16-mercaptohexadecanoic acid (MHA), ascorbic acid,

triethylamine, oleoyl chloride, and (*S*)-(+)-camptothecin (CPT) were obtained from

Sigma-Aldrich, Japan (Tokyo, Japan). Hoechst33342 and LysoTracker Green DND-26

were obtained from Invitrogen (Oregon, USA). Doxorubicin hydrochloride (DOX·HCl)

was purchased from Kyowa Hakko Kirin Co., Ltd. (Tokyo, Japan). Dimethylsulfoxide

(DMSO), N,N'-dimethylformamide (DMF) and calcium oxide were supplied from

Kishida Chemical (Osaka, Japan). DMSO was used after the distillation. α-methoxy-ω-

(p-nitrophenylcarbonate) PEG (PEG-NPC) was synthesized as reported[30].

2.2. Preparation of Dendrimer−AuNR, Oleoyl−Dendrimer−AuNR.

AuNR with the aspect ratio of 4 were prepared through seedless method to provide

them with the NIR responsiveness. In addition, carboxy group was incorporated by ligand

exchange reaction from CTAB to MHA (Scheme 1, See supporting information).

Dendrimer−AuNR was synthesized by conjugation of PEG-attached PAMAM G4

dendrimer with MHA−AuNR through the condensation reaction between primary amine of PEG-attached PAMAM dendrimer and carboxy group of MHA−AuNR using EDC/NHS. MHA−AuNR dispersion (10 mg, 10 mL) was added to PEG−PAMAM in phosphate buffered saline (PBS) (20 mg, 5 mg/mL). After the pH adjustment to 8.0 using HCl, EDC (3.6 mg) and NHS (1.1 mg) aqueous solution were added and then the solution was sonicated for 2 h at 4 °C using bath-type sonicator. The mixture was stirred overnight at room temperature. Excess reagents were removed by centrifugation (14,000 rpm, 15 min) and redispersed in DMF for the following synthesis or in PBS for other measurements.

Introduction of oleoyl groups into amino groups of PAMAM dendrimer on AuNR was performed as follows: oleoyl chloride (4.2 mg) solution in DMF and triethylamine (2.9 mg) was added to Dendrimer−AuNR dispersion in DMF (3 mL, 10 mg) and stirred for 3 h at room temperature. Then, reaction solution was centrifuged (15,000 rpm, 15 min) twice to remove unreacted oleoyl chloride. Obtained Oleoyl−Dendrimer−AuNR (nanohybrids) was redispersed in PBS.

2.3. General characterization of PEG-dendrimer and nanohybrids.

The absorption spectra of the each as-prepared AuNRs were analyzed using a Jasco V-670 spectrophotometer (Jasco Inc., Tokyo, Japan) at a wavelength range of 400-1100 nm. Au concentration of each sample was determined using SPS7800 ICP-MS spectrometer (Seiko Instruments Inc., Chiba, Japan). Diameters of the PEG-dendrimer in 0.1 mM phosphate aqueous solution were measured using a Zetasizer Nano ZS ZEN3600 (Malvern Instruments Ltd, Worcester-shire, UK). Surface morphology of as-synthesized AuNRs was analyzed using transmission electron microscopy (TEM) (JEOL Ltd., JEM-2000FEX II, Tokyo, Japan) operated at 200 kV. Before TEM observation, the dispersion was dropped on a carbon-coated copper grid, and then excess of dispersion was removed with a filter paper. Then 20 µL of 2% aqueous sodium phosphotungstate solution was dropped on a grid and dried in a desiccator overnight. The composition of organic compounds bound to as-synthesized AuNR was assessed by thermal gravimetric analysis (STA-7200, Hitachi, Ltd. Tokyo, Japan)). Dendrimer−AuNR, Oleoyl−Dendrimer−AuNR, MHA−AuNR dispersion were centrifuged (15,000 rpm, 20 min) and washed with distilled water several times and each residue was dried under vacuum. Each dried sample was collected and heated from room temperature to 700 °C at a heating rate of 10 °C/min and calibrated using Pt as a standard sample.

2.4. Photothermal properties.

Nanohybrid (Oleoyl−Dendrimer−AuNR) dispersion of a given concentration of Au (2.3 µg/mL, 4.5 µg/mL and 45 µg/mL, 1 mL) in DMEM suppremented with 10% FBS without phenol red was placed in a quartz cell. NIR laser (YHTC Co., Ltd, KLD-3ALT, λ = 808 nm, 6 W/cm^2, Tokyo, Japan) was irradiated to nanohybrid dispersion, in which initial temperature of the dispersion was fixed to be 27°C, and the change in temperature of the dispersion was monitored using a thermometer (SK-1250MC, SATO KEIRYOKI MFG. Co., Ltd, Tokyo, Japan). In addition, the temperature change was also monitored when a pulsed laser (a pulse width was 10 min with 15 min interval) was irradiated to dispersion.

2.5. Drug loading and release.

Loading of DOX into nanohybrids was performed by adding DOX aqueous solution to nanohybrids dispersion in PBS (pH 7.4) so as to be various DOX/Au (wt/wt) ratios (0.015, 0.030, 0.045 and 0.061). After overnight storage under dark, DOX-loaded nanohybrids were purified by two cycles of centrifugation at 15,000 rpm for 20 min. To determine DOX loading efficacy, DOX/Dendrimer−AuNR or DOX/Oleoyl−Dendrimer−AuNR was dissolved in acidified isopropanol (0.75 M HCl in

isopropanol)[34,35]. DOX was released from DOX/Dendrimer−AuNR or DOX/Oleoyl−Dendrimer−AuNR by acidified isopropanol. After the separation by centrifugation (15,000 rpm, 30 min). The loaded amount of DOX was calculated at the absorption at 495 nm by subtracting the DOX amount in the supernatant from the amount of DOX initially added to nanohybrids. The loading of CPT into nanohybrid was performed by similar procedure with DOX loading. CPT dissolved in DMF (0.2 mL, 6.1 μg/mL) was added to nanohybrid dispersion in pH 7.4 PBS (0.8 mL, 0.025 mg/mL) at CPT/Au ratio of = 0.061 wt/wt. After overnight storage under dark, The solution was evaporated and dried under vacuum to remove water and DMF. The obtained compound was dissolved in pH 7.4 PBS and centrifuged at 15,000 rpm for 20 min to remove unloaded CPT. The CPT concentration in the supernatant was determined by fluorescence measurement, in which excitation and emission wavelengths for CPT were 370 nm and 434 nm.

The drug loading content (LC) and loading efficiency (LE) were determined according to the following formula:

$$LC\ (wt\%) = \frac{\text{weight of loaded drug}}{\text{total weight of nanohybrids and loaded drug}} \times 100$$

$$LE\ (\%) = \frac{\text{weight of loaded drug}}{\text{weight of drug in feed}} \times 100$$

DOX or CPT release from drug-loaded nanohybrids was estimated in PBS (pH 7.4 or 5.0) using a dialysis method. An aliquot (1 mL) of drug-loaded nanohybrids suspension was loaded in a dialysis bag (molecular weight cut off: 12,000-14,000). The dialysis bag was immediately immersed in 100 mL of corresponding buffer at 4 °C. The external buffer solutions were collected from the dialysis cassette at predetermined times. Drug concentration in the collected samples were determined by fluorescence measurement, in which excitation and emission wavelengths for DOX were 468 nm and 590 nm, and excitation and emission wavelengths for CPT were 370 nm and 434 nm.

2.6. *In vitro* cytotoxicity assay.

Human cervix adenocarcinoma-derived HeLa cells were grown in DMEM supplemented with 10% FBS (MP Biomedical, Santa Ana, USA) and antibiotics at 37 °C under 5% CO_2 condition. HeLa cells were seeded into a 96-well microplate (1×10^4 cells/well) in 100 μL of DMEM supplemented with 10% FBS and cultured for 24 h. 20 μL of DOX/Oleoyl–Dendrimer–AuNR, CPT/Oleoyl–Dendrimer–AuNR, DOX/Dendrimer–AuNR, CPT/Dendrimer–AuNR, free DOX or free CPT at various concentrations in PBS (pH 7.4) were gently added to the cells and incubated for 3 h. Cells were gently washed with PBS twice, and incubated for another 21 h in 100 μL of DMEM

supplemented with 10% FBS. Cells were then irradiated with NIR laser from the top of the plate at a power density of 6.0 W/cm^2 for 10 min. Cells without irradiation were used as a control. After irradiation treatment, cells were cultured for another 24 h. The culture medium was then replaced with DMEM with 10% FBS containing MTT. 3 h after incubation, the medium was removed, and the cells were solubilized in isopropanol containing 0.1 M HCl. The viable cells were counted from the absorbance at 490 nm using Microplate Reader (SH-8000 CORONA ELECTRIC Co., Ltd., Ibaraki, Japan).

2.7. Confocal laser scanning microscopy.

HeLa cells (2×10^5 cells) were seeded into a 35 mm glass-bottom dish in 2 mL of DMEM supplemented with 10% FBS and cultured for 24 h. 200 μL of free DOX solution or DOX-loaded nanohybrids dispersion in PBS was added (1 μg DOX/mL). After 1 h-incubation, cells were gently washed with PBS twice, and incubated for 2 h in DMEM supplemented with 10% FBS, followed by addition of 30 μL of LysoTracker Green DND-26 (10 pmol/μL) and 1 μL of Hoechst33342 (10 mg/mL). After 15 min staining, cells were washed with PBS three times. Confocal laser scanning microscopic (CLSM) analysis of these cells was performed using LSM 5 EXCITER (Carl Zeiss Co., Ltd., Oberkochen, Germany).

2.8. Animals.

Seven-weeks-old female BALB/c mice were purchased from Oriental Yeast Co., Ltd. (Tokyo, Japan). Experiments were carried out in accordance with the guidelines for animal experimentation in Osaka Prefecture University.

2.9. *In vivo* antitumor efficacy.

Antitumor effect of DOX-loaded nanohybrids (DOX/Oleoyl−Dendrimer−AuNR) was examined according to both intravenous and intratumoral injection methods. Laser power density and injection dosage were reduced comapared with *in vitro* assay to avoid the heat injury by NIR laser irradiation in a viewpoint of animal care. Colon carcinoma 26 cells were grown in RPMI-1640 supplemented with 10% FBS and antibiotics at 37 °C under 5% CO_2. Tumor-bearing mice were prepared by inoculating colon 26 cells (1×10^6 cells) into the right flank of BALB/c mice (female, 7 weeks old) under anesthesia using isoflurane and the tumor was allowed to grow for about 7-10 days, when the tumor volume was approximately 100 mm^3. An aliquot (100 μL) of DOX-loaded nanohybrids (containing 0.45 mg of Au element with/without 10 μg DOX) or PBS was intravenously injected into the mice under anesthesia (n = 3-4 per group). At 24 h after injection, the

entire region of tumor was irradiated with NIR laser at 2.3 W/cm^2 for 10 min. For intratumoral injection method, an aliquot (100 μL) of DOX-loaded nanohybrids (containing 0.2 mg of Au element with/without 4 μg DOX) or PBS was intratumorally injected into the mice under anesthesia (n = 3-4 per group). After sample injection, the entire region of tumor was immediately irradiated with NIR laser at 1.5 W/cm^2 for 10 min. During irradiation, thermographs were taken using a NIR camera (InfReC Thermograph yR300, Nippon Avionics, Co., Ltd., Tokyo, Japan). The thermographs were analyzed to obtain the maximum temperature at each time point. Tumor volumes were monitored and calculated using the following formula:

Tumor volume = $(L \times W^2) / 2$

where L is the longest dimension parallel to the skin surface and W is the dimension perpendicular to L and parallel to the surface.

2.10. Statistical analysis.

Student's t-test (Fig. 3A, S4) or Tukey-Kramer-test (Figs. 6D and S11D) were employed for the statistical evaluation of the results.

3. Results and discussion

3.1. Nanohybrid characterization

Dendrimer–AuNR was prepared as reported earlier (see Supporting information)[30]. Furthermore, oleoyl group was incorporated using a reaction of oleoyl chloride with the remaining amino groups of PAMAM dendrimer (Scheme 1). The organic component composition of nanohybrids was analyzed using TGA (Figure 2A). Based on TGA, the average numbers of PEG-dendrimer molecules per AuNR and oleoyl groups per PEG-dendrimer were quantified respectively as 12 and 42 (see Supporting information). According to DLS measurements, the hydrodynamic diameter of PEG-dendrimer was 18 nm. Considering that dendrimers are packed with the surface of AuNR, the maximum number of PEG-dendrimer is inferred as 29 (Table S1, see Supporting information). Differences between TGA results and calculations suggest that PEG dendrimers densely cover the gold nanorod surface with interdigitation between PEG layers (Figure S1B). Furthermore, as shown in Table S1, ^{1}H NMR analysis revealed that almost all amino groups were reacted with oleoyl chloride.

Next, we investigated the photothermal properties of nanohybrids, absorption spectra, and thermal behavior. As shown in Figure 2B, nanohybrids showed strong absorption around 808 nm corresponding to LSPR for conversion of heat from NIR light energy. Conjugation of dendrimers did not change the peak or the absorption coefficient.

Photothermal conversion efficiency of nanohybrid was calculated as 24.8% (see Supporting information), which is consistent with representative photothermal conversion efficiency of AuNR[16]. This indicates that photothermal conversion property of AuNR was maintained even after conjugation of oleoyl group-introduced PEG-dendrimers. Figure 2C shows photothermal behavior of nanohybrid dispersion in cell culture medium upon NIR light irradiation at 808 nm. The nanohybrid dispersion temperature increased concomitantly with time depending on the Au concentration, whereas DMEM supplemented with 10% FBS (0 μg/mL) showed no marked temperature change under laser irradiation. Figure 2D shows that the stability of photothermal behavior of nanohybrid was also investigated. Photothermal behavior didn't change through repeated cycles of ON/OFF of NIR light irradiation, indicating that nanohybrids are stable at increased temperatures and under exposure to continuous NIR laser light. Hydrated PEG chains covering AuNR might provide high colloidal stability and might therefore affect the stable photothermal properties by avoidance of aggregation during repeated exposure to NIR light.
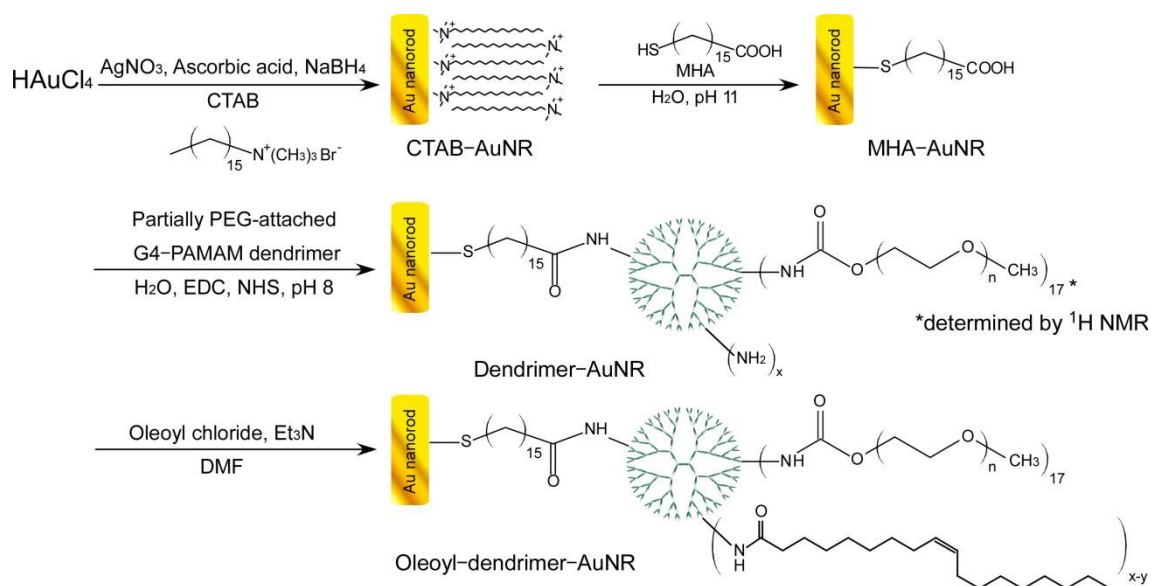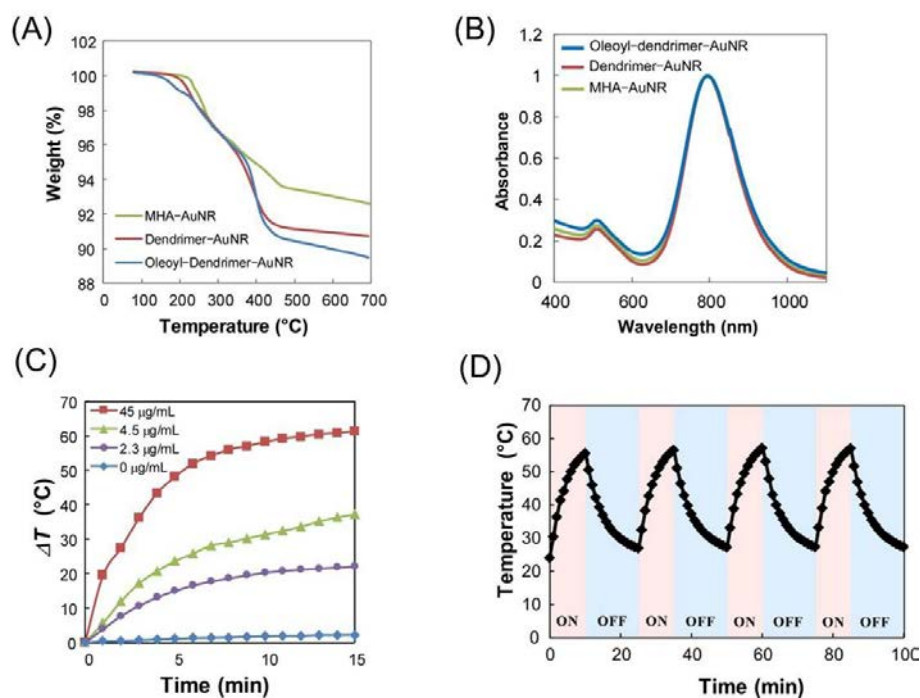
Scheme 1. Nanohybrid preparation.

Figure 2. Characterization of nanohybrids: (A) TGA curves of MHA–AuNR, dendrimer–

AuNR, and oleoyl-dendrimer–AuNR; (B) absorption spectra of MHA–AuNR,

dendrimer–AuNR, and oleoyl-dendrimer–AuNR. Whereas MHA–AuNR was dispersed

19

in pH 11.5 distilled water, dendrimer–AuNR and oleoyl–dendrimer–AuNR were dispersed in pH 7.4 PBS. (C) Photoirradiation-induced increase in temperature of aqueous solutions of nanohybrids. The initial temperature was 27 °C. (D) Change in temperature increase of nanohybrids ($[Au] = 4.5$ μg/mL) for four NIR laser on/off cycles ($\lambda = 808$ nm, 6 W/cm^2).

3.2. Drug loading and release

Next, dendrimer–AuNR and oleoyl–dendrimer–AuNR drug loading amounts were compared to evaluate the drug encapsulation efficacy achieved through hydrophobic interaction of oleoyl chains. Nanohybrids loaded with DOX or CPT (Figure S3) were prepared by mixing nanohybrid dispersion and drug solution in PBS. Excess drugs were removed by repeated centrifugation. Figure 3A shows the relation between feed DOX and encapsulated DOX in nanohybrids. Loaded DOX in the nanohybrid increased along with the DOX feeding amount, but it reached a plateau at a high concentration of the feed DOX. Results show that the DOX loading capacity was increased considerably by incorporation of oleoyl chains to PEG-dendrimer in the nanohybrid. The doxorubicin molecules per dendrimer or oleoyl-dendrimer were, respectively, 65 and 110. Incorporating oleoyl chains increased the loading efficiency (LE) from 20.0±0.2% to 36.0±3.9% (Table S2).

The loading content (LC) also increased from 1.2±0.1% to 2.2±0.2%. Figure S4 shows the amounts of DOX or CPT loaded in PEG–dendrimer–AuNR nanohybrids with or without oleoyl chains (drug/Au in feed is 0.061 mg/mg). The amount of loaded CPT slightly changed in the case of nanohybrid with oleoyl chain: LC was almost identical from 1.5±0.1% to 1.6±0.1% and LE slightly changed from 24.7±1.6% to 27.1±1.4% (Table S2). The water solubility of CPT is relatively low compared with DOX. During the dispersion in PBS after removal of CPT/DMF and PEG–dendrimer–AuNR nanohybrids/water might promote the precipitation of CPT rather than loading into nanohybrids via hydrophobic interaction, resulting in almost identical drug loading irrespective with oleoyl group introduction.

Free DOX diffused rapidly through the dialysis membrane, whereas nanohybrids gradually released DOX, probably because of interaction with PEG–dendrimer (Figure 3B). The DOX release rate from nanohybrids at pH 5.0 was much higher than at pH 7.4. Considering that the pKa of amino group of DOX is about 7.0[39,40], protonation of amino groups of DOX in acidic pH changed the aqueous solubility, which promoted DOX release from nanohybrids. Probably because of high concentration gradient of inside and outside of dialysis membrane, no significant difference was found in release with/without the oleoyl chain. The release of CPT from both nanohybrids was about 40% after 7 h

incubation at any pH because of a lack of protonation of quinoline of CPT having pKa of 1.2 (Figure S5)[41]. The effect of temperature change on drug release by laser irradiation or thermal heating using a peltier instrument was also evaluated (Figure S6). NIR laser irradiation (15 min, 6 W/cm^2) promoted DOX release amount from DOX/Oleoyl-dendrimer-AuNR dispersion compared with the cases of without treatment (just 15 min incubation at room temperature) or external heating application using a peltier instrument. These results suggest that local heating surrounding AuNR by NIR laser irradiation promotes the drug molecular motion locally, leading to the increased drug release.
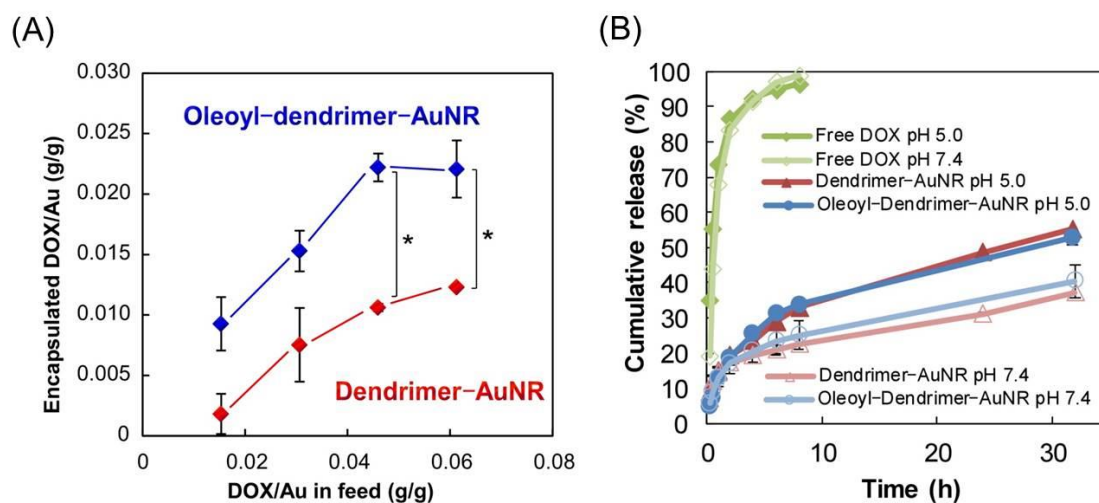

Figure 3. (A) Amount of DOX incorporated into PEG–dendrimer–AuNR nanohybrids with or without oleoyl chains as a function of DOX/Au ratio in feed (g/g). (B) Release profiles of DOX from dendrimer–AuNR or oleoyl–dendrimer–AuNR in PBS of pH 7.4 or pH 5.0. *$p < 0.01$.

3.3. *In vitro* cellular interaction using DOX-loaded nanohybrids

Cancer cell killing effects of nanohybrid were investigated *in vitro*. As shown in Figure S7A, oleoyl–dendrimer–AuNR exhibited superior cancer-cell killing efficacy when compared in same Au concentration. This might result from its improved loading capacity by incorporation of oleoyl chains to PEG–dendrimer of the nanohybrid (Figure 3A) and because of its DOX release rate, which was unchanged irrespective of the existence of oleoyl chain (Figure 3B). Cell viability was also compared in same DOX concentration (Figure S7B). Oleoyl–dendrimer–AuNR also showed slightly high cytotoxicity compared with dendrimer–AuNR, which might result from increase cellular association of nanohybrids via hydrophobic interaction derived from oleoyl chains. Therefore, oleoyl–dendrimer-based nanohybrids were used for the following experiments. Incubation of non-DOX-loaded nanohybrids with cells showed negligible cytotoxicity irrespective of the Au concentration, but combination of a non-DOX-loaded nanohybrid with laser irradiation markedly decreased cell viability depending on the Au concentration (Figure 4), which might indicate that heat generation from nanohybrids under laser irradiation is sufficient to induce cancer cell death. Actually, DOX/oleoyl–dendrimer–AuNR showed dose-dependent cytotoxicity, but its cytotoxicity was lower

than that of free DOX (Figure 4), perhaps because of the difference in DOX molecule

uptake mechanisms, as discussed later with respect to CLSM analysis. When HeLa cells

were incubated with DOX-loaded nanohybrids and irradiated by NIR laser, cell viability

decreased drastically: it became lower than that achieved using DOX/oleoyl–dendrimer–

AuNR without laser light and using oleoyl–dendrimer–AuNR with laser light. These

results demonstrate that nanohybrids have strong cell-killing capability through the

synergy of DOX-induced chemo effect and AuNR-induced photothermal effect. CPT-

loaded nanohybrids also showed dose-dependent cytotoxicity (Figure S8). Both

Dendrimer-AuNR and Oleoyl-Dendrimer-AuNR did not show any cytotoxicity in the

experimental concentration condition, whereas laser irradiation significantly reduced the

cell viability. But cell-killing effects of both nanohybrids with laser irradiation were less

than those of CPT-loaded nanohybrids. Therefore, CPT-loaded nanohybrids also showed
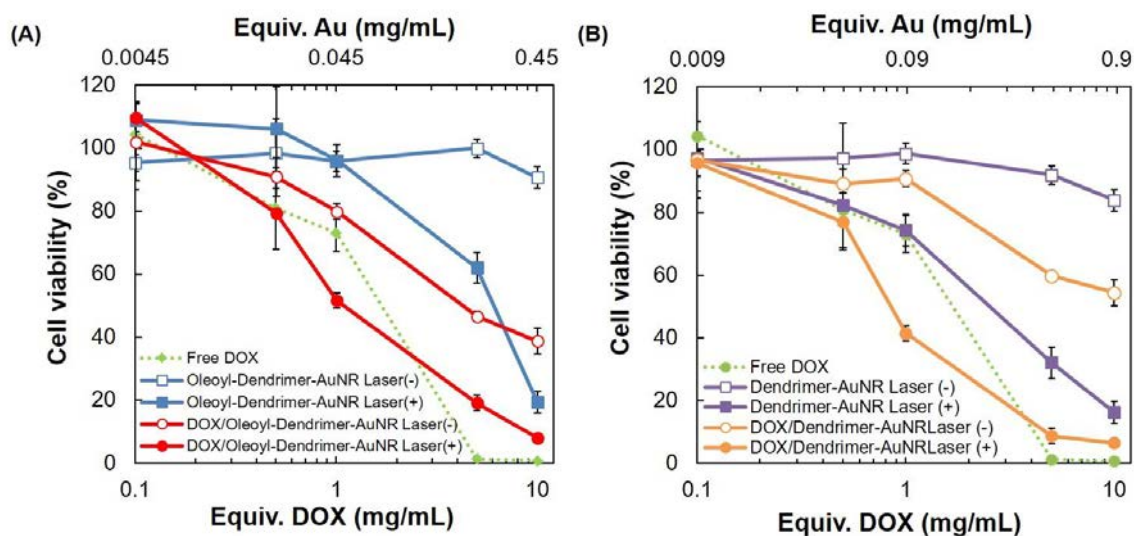
synergy of chemo effect and photothermal effect.

Figure 4. Dependence of cell viability on DOX concentration for HeLa cells treated with (A) oleoyl–dendrimer–AuNR with or without DOX or dendrimer–AuNR with or without DOX (DOX). Free DOX was also used as a control. After 3 h incubation, cells were irradiated with or without NIR laser (λ = 808 nm, 6 W/cm^2, 10 min).

To ascertain the intracellular distribution and cell uptake behavior of DOX-loaded nanohybrids, CLSM observations were conducted (Figure 5). First, DOX/oleoyl–dendrimer–AuNR was incubated with HeLa cells for 1 h. The fluorescence of DOX and LysoTracker were observed at 2 h after additional incubation. When treated with free DOX, the DOX fluorescence was observed from the nucleus. Free DOX is known to penetrate the cell membrane and to accumulate into the nucleus through intercalation to DNA, resulting in strong cytotoxicity compared with DOX/oleoyl–dendrimer–AuNR without laser irradiation (Figure S9). However, punctate fluorescence of DOX overlying

that of LysoTracker was observed for HeLa cells treated with DOX-loaded nanohybrids.

Considering that surface energy transfer (SET) quenched the fluorescence of DOX

(Figure S10)[21], HeLa cells might take up nanohybrids through endocytosis and release

DOX in endosomes or lysosomes. Nanohybrids showed cytotoxicity against HeLa cells.

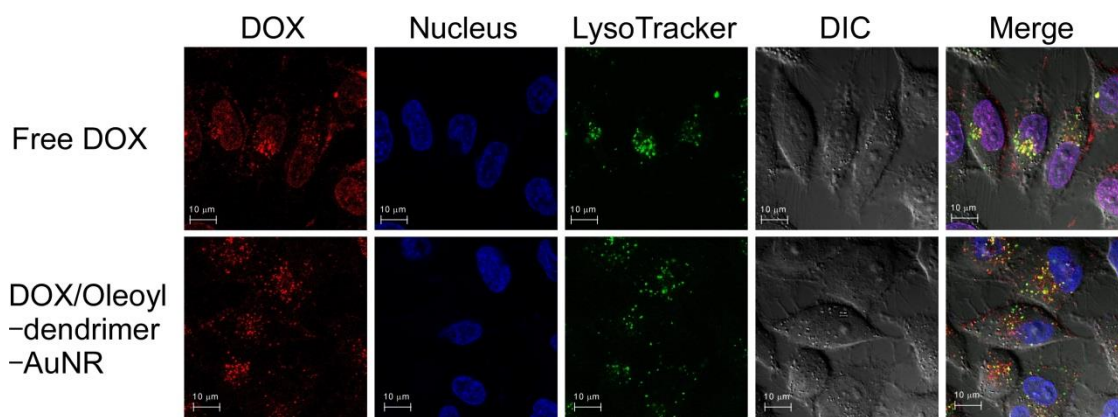Therefore, the released DOX can be expected to reach the nucleus eventually (Figure S9).

Figure 5. CLSM images of HeLa cells treated with free DOX or DOX/oleoyl–dendrimer–

AuNRs for 1 h at 37 °C in the presence of 10% serum. After washing with PBS, cells

were incubated for 2 h. Then acidic compartments and nuclei of HeLa cells were stained

respectively using LysoTracker green and Hoechst 33342.

3.4. *In vivo* antitumor effects

Finally, therapeutic effects of DOX-loaded nanohybrids *in vivo* were investigated.

Firstly, DOX/oleoyl–dendrimer–AuNR was injected intravenously to tumor-bearing

mice. Thermographs were taken during NIR light irradiation using a thermal camera to confirm the photothermal effect of AuNRs. Figure S11B shows typical thermographs of nanohybrid-treated or PBS-treated mice with 0, 2, and 5 min laser irradiation to a tumor at 24 h after intravenous injection. In nanohybrid-injected mice, the whole-tumor temperature increased to more than 46 °C 5 min after NIR laser irradiation, which can engender thermoablation[42]. The high temperature increase in nanohybrid-injected mice indicates the accumulation of nanohybrids to the tumor site through EPR effects[43,44] and the generation of heat mediated by LSPR of AuNR. Figure S11C shows the temperature change of the tumor region under laser irradiation. During 10 min of laser irradiation, tumors of mice injected with DOX/oleoyl–dendrimer–AuNR and oleoyl–dendrimer–AuNR had maximum temperatures of 47.8 °C and 48.5 °C respectively, whereas a similarly irradiated PBS-treated tumor showed an average temperature of 41.9 °C, which is insufficient to induce thermal damage to tumor cells. Figure S11D shows tumor volume changes achieved under various treatments. Injection of 10 μg of DOX, which corresponds to DOX amounts in DOX-loaded nanohybrids, showed no antitumor effect. In contrast, intravenous injection of DOX/oleoyl-dendrimer–AuNR suppressed tumor growth slightly, which suggests that the accumulation of nanohybrids and subsequent DOX release at the tumor site can improve the antitumor effects of DOX. Furthermore, a

combination of NIR laser irradiation and nanohybrids with/without DOX achieved significantly better suppression of tumor growth than that achieved with other treatment groups (Figure S11D), which indicates that the high temperature increase over the whole tumor area efficiently induced tumor cell killing effects even in the absence of DOX in nanohybrids.

In the case of intravenous injection, photothermal effect via laser-irradiated nanohybrids was dominant compared with DOX-chemo effect. As another treatment method, antitumor effects through intratumoral injection were also examined (Figure 6). According to the thermographs under NIR laser irradiation, the temperature in the irradiated area immediately increased to around 50 °C (Figures 6B and 6C). However, the highly heated area was narrower than in cases of intravenous injection (Figure 6B and Figure S11B). Nanohybrids might be localized near the injection site, leading to immediate and high temperature increases within localized areas. Intratumoral injection of free DOX and DOX/oleoyl-dendrimer–AuNR showed moderate antitumor effects (Figure 6D). By contrast, because of the greatly increased temperature under NIR laser irradiation, the combination of NIR laser irradiation of nanohybrids showed markedly superior antitumor effects to those of nanohybrids without laser irradiation (Figures 6C and 6D). Especially, tumor growth of DOX/oleoyl-dendrimer–AuNR + laser was

suppressed almost completely, although the tumor grew gradually in the case of oleoyl-dendrimer–AuNR + laser. Nanohybrids without DOX were able to kill tumor cells at localized heating areas, but remaining cells in peripheral areas might gradually grow. The DOX/oleoyl–dendrimer–AuNR + laser treatment induced a strong tumor cell killing effect under laser irradiation in the localized area. Moreover, DOX released from nanohybrids induced tumor cell apoptosis in peripheral areas, thereby suppressing tumor growth almost completely. These results suggest the importance of combining DOX-derived chemo effects and AuNR-derived photothermal effects to achieve effective cancer treatment. In addition, any remarkable body weight changes during all *in vivo* experiments were not observed (Figure S12).
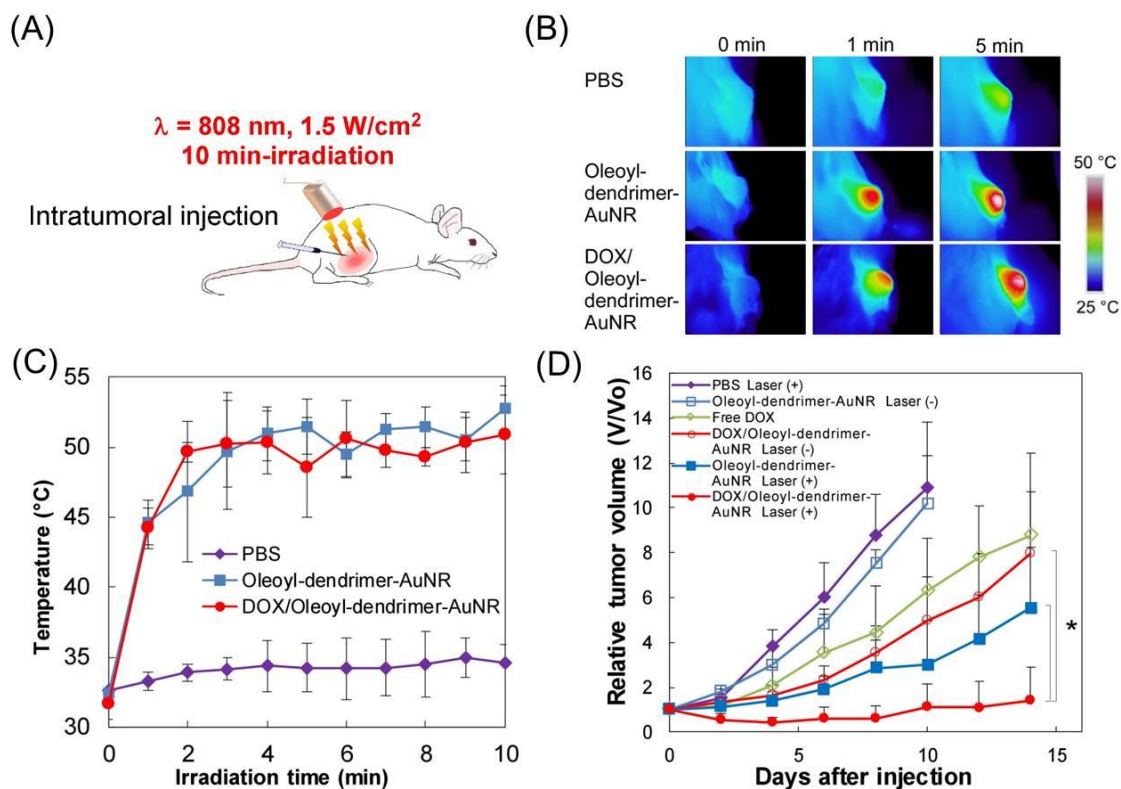
Figure 6. (A) Experimental representation of nanohybrid treatment achieved using intratumoral injection with NIR light irradiation for colon-26-bearing mice. (B) Thermographs of DOX-loaded nanohybrid and PBS intratumorally injected mice receiving photothermal treatment for different periods of time. (C) Time courses of temperature variation in the right tumor region under NIR laser irradiation ($\lambda = 808$ nm, 1.5 W/cm^2) after intratumoral injection with PBS, DOX-unloaded nanohybrids, or DOX-loaded nanohybrids. (D) Tumor growth profiles of tumor-bearing mice after intratumoral injection of DOX-unloaded nanohybrid, DOX-loaded nanohybrid (0.2 mg Au and 4 μg DOX) or PBS with/without NIR laser irradiation (808 nm, 1.5 W/cm^2, 10 min). Tumor volumes were normalized to their initial sizes. *$p < 0.01$.

30

4. Conclusions

Functional dendrimer and gold nanorod-based nanohybrids were prepared to induce synergistic cancer treatment effects attributable to an anticancer drug and laser hyperthermia. To improve anticancer drug loading, oleoyl chains were introduced to PEG-dendrimer. The obtained nanohybrids showed heat generation under NIR laser irradiation and gradual drug release. Combinations of DOX-loaded nanohybrids and laser irradiation exhibited strong cell killing capability both *in vitro* and *in vivo* through the synergy of DOX-induced chemo effect and AuNR-induced photothermal effect. Results show that functional dendrimer and gold nanorod-based nanohybrids are promising as a platform for multi-functional nanomaterials to achieve effective cancer therapy.

Supporting information

Supporting information is available free of charge at http://

Calculation of the number of PEG-dendrimers and oleoyl groups in Oleoyl−Dendrimer−AuNR. Synthetic route of PEG−PAMAM dendrimer. Characterization of nanohybrids. Calculation of the photothermal efficiency. Drug

loading and release of CPT. Effect of heatin on drug release. Cell viability of HeLa cells treated with DOX- or CPT-loaded nanohybrids. Fluorescence spectra of Free DOX, Free DOX + CTAB−AuNR, DOX/Oleoyl−Dendrimer−AuNR. *In vivo* antitumor effect of nanohybrid through intravenous injection. Body weight changes for *in vivo* experiments.

References

1 A. C. Steger, W. R. Lees, K. Walmsley and S. G. Bown, *BMJ*, 1989, **299**, 362–365.

2 N. Frazier and H. Ghandehari, *Biotechnol. Bioeng.*, 2015, **112**, 1967–1983.

3 L. Dykman and N. Khlebtsov, *Chem. Soc. Rev.*, 2012, **41**, 2256–2282.

4 Y. Bayazitoglu, S. Kheradmand and T. K. Tullius, *Int. J. Heat Mass Transf.*, 2013, **67**, 469–486.

5 X. H. Huang, I. H. El-Sayed, W. Qian and M. A. El-Sayed, *J. Am. Chem. Soc.*, 2006, **128**, 2115–2120.

6   X. Huang, P. K. Jain, I. H. El-Sayed and M. A. El-Sayed, *Lasers Med. Sci.*, 2008, **23**, 217–228.

7   G. Kandasamy and D. Maity, *Int. J. Pharm.*, 2015, **496**, 191–218.

8   C. Liang, S. Diao, C. Wang, H. Gong, T. Liu, G. Hong, X. Shi, H. Dai and Z. Liu, *Adv. Mater.*, 2014, **26**, 5646–5652.

9   F. Zhou, D. Xing, Z. Ou, B. Wu, D. E. Resasco and W. R. Chen, *J. Biomed. Opt.*, 2009, **14**, 021009.

10   W.-F. Cheong, S. A. Prahl and A. J. Welch, *IEEE J. Quantum Electron.*, 1990, **26**, 2166–2185.

11   R. Weissleder, *Nat. Biotechnol.*, 2001, **19**, 316–317.

12   L. Zou, H. Wang, B. He, L. Zeng, T. Tan, H. Cao, X. He, Z. Zhang, S. Guo and Y. Li, *Theranostics*, 2016, **6**, 762-772.

13   A. M. Alkilany, L. B. Thompson, S. P. Boulos, P. N. Sisco and C. J. Murphy, *Adv. Drug Deliv. Rev.*, 2012, **64**, 190–199.

14   E. Locatelli, I. Monaco and M. Comes Franchini, *RSC Adv.*, 2015, **5**, 21681–21699.

15   A. S. D. S. Indrasekara, R. C. Wadams and L. Fabris, *Part. Syst. Charact.*, 2014, **31**, 819–838.

16   W. Fan, B. Yung, P. Huang and X. Chen, *Chem. Rev.*, 2017, **117**, 13566–13638.

17   P. Huang, L. Bao, C. Zhang, J. Lin, T. Luo, D. Yang, M. He, Z. Li, G. Gao, B. Gao, S. Fu and D. Cui, *Biomaterials*, 2011, **32**, 9796–9809.

18   C. Li, Y. Zhang, Z. Li, E. Mei, J. Lin, F. Li, C. Chen, X. Qing, L. Hou, L. Xiong, H. Hao, Y. Yang and P. Huang, *Adv. Mater.*, 2018, **30**, 1706150.

19   C.-C. Chen, Y.-P. Lin, C.-W. Wang, H.-C. Tzeng, C.-H. Wu, Y.-C. Chen, C.-P. Chen, L.-C. Chen and Y.-C. Wu, *J. Am. Chem. Soc.*, 2006, **128**, 3709–3715.

20   S. Shen, H. Tang, X. Zhang, J. Ren, Z. Pang, D. Wang, H. Gao, Y. Qian, X. Jiang and W. Yang, *Biomaterials*, 2013, **34**, 3150–3158.

21   R. Venkatesan, A. Pichaimani, K. Hari, P. K. Balasubramanian, J. Kulandaivel and K. Premkumar, *J. Mater. Chem. B*, 2013, **1**, 1010–1018.

22   C. G. Wilson, P. N. Sisco, F. A. Gadala-Maria, C. J. Murphy and E. C. Goldsmith, *Biomaterials*, 2009, **30**, 5639–5648.

23   J. Zhou, Z. Cao, N. Panwar, R. Hu, X. Wang, J. Qu, S. C. Tjin, G. Xu and K.-T. Yong, *Coord. Chem. Rev.*, 2017, **352**, 15–66.

24   N. Taghavi Pourianazar, P. Mutlu and U. Gunduz, *J. Nanoparticle Res.*, 2014, **16**, 2342.

25   H. Maeda, *Adv. Drug Deliv. Rev.*, 2015, **91**, 3–6.

26   A. K. Sharma, A. Gothwal, P. Kesharwani, H. Alsaab, A. K. Iyer and U. Gupta, *Drug Discov. Today*, 2017, **22**, 314–326.

27   E. Pérez-Herrero and A. Fernández-Medarde, *Eur. J. Pharm. Biopharm.*, 2015, **93**, 52–79.

28   A.-M. Caminade and C.-O. Turrin, *J. Mater. Chem. B*, 2014, **2**, 4055–4066.

29   K. Gavvala, A. Sengupta and P. Hazra, *ChemPhysChem*, 2013, **14**, 532–542.

30   X. Li, M. Takashima, E. Yuba, A. Harada and K. Kono, *Biomaterials*, 2014, **35**, 6576–6584.

31   A. D'Emanuele and D. Attwood, *Adv. Drug Deliv. Rev.*, 2005, **57**, 2147–2162.

32   C. Kojima, Y. Toi, A. Harada and K. Kono, *Bioconjug. Chem.*, 2007, **18**, 663–670.

33   K. Kono, T. Fukui, T. Takagishi, S. Sakurai and C. Kojima, *Polymer.*, 2008, **49**, 2832–2838.

34   I. Matai and P. Gopinath, *RSC Adv.*, 2016, **6**, 24808–24819.

35   C. Kojima, C. Regino, Y. Umeda, H. Kobayashi and K. Kono, *Int. J. Pharm.*, 2010, **383**, 293–296.

36   T. Niidome, M. Yamagata, Y. Okamoto, Y. Akiyama, H. Takahashi, T. Kawano, Y. Katayama and Y. Niidome, *J. Control. Release*, 2006, **114**, 343–347.

37   K. M. Laginha, S. Verwoert, G. J. R. Charrois and T. M. Allen, *Clin. Cancer Res.*, 2005, **11**, 6944–6949.

38   Y. Zhong, C. Wang, L. Cheng, F. Meng, Z. Zhong and Z. Liu, *Biomacromolecules*, 2013, **14**, 2411–2419.

39   S. Eksborg, *J. Pharm. Sci.*, 1978, **67**, 782–785.

40   K. Kataoka, T. Matsumoto, M. Yokoyama, T. Okano, Y. Sakurai, S. Fukushima, K. Okamoto and G. S. Kwon, *J. Control. Release*, 2000, **64**, 143–153.

41   K. Gavvala, A. Sengupta and P. Hazra, *ChemPhysChem*, 2013, **14**, 532–542.

42   C. S. S. R. Kumar and F. Mohammad, *Adv. Drug Deliv. Rev.*, 2011, **63**, 789–808.

43   H. Maeda, J. Wu, T. Sawa, Y. Matsumura and K. Hori, *J. Control. Release*, 2000, **65**, 271–284.

44   H. Maeda, *Adv. Drug Deliv. Rev.*, 2015, **91**, 3–6.